Structure of one-dimensional monolayer Si nanoribbons on Ag(111)

Lingyu Feng,[1] Akitoshi Shiotari,[1] Keisuke Yabuoshi,[1] Masahiro Fukuda,[2] Taisuke Ozaki,[2] and Yoshiaki Sugimoto[1,*]
[1]*Department of Advanced Materials Science, The University of Tokyo, 5-1-5 Kashiwanoha, Kashiwa, Chiba 277-8561, Japan*
[2]*Institute for Solid State Physics, The University of Tokyo, 5-1-5 Kashiwanoha, Kashiwa, Chiba 277-8581, Japan*

(Received 6 October 2020; revised 22 January 2021; accepted 23 February 2021; published 9 March 2021)

One-dimensional silicon nanoribbons (SiNRs) have the potential for application to future electronic devices because of their compatibility with current silicon-based electronic devices and their theoretical outstanding electronic properties, such as the size-dependent band gap. Here we grew SiNRs by the deposition of Si on a Ag(111) surface. We investigated SiNRs on the Ag(111) surface using a combination of scanning tunneling microscopy (STM), atomic force microscopy (AFM), and density functional theory (DFT) calculations. The atomic resolution STM and AFM images revealed that SiNRs have the same width and align along the equivalent orientations of Ag(111). The main body of SiNRs was found to be symmetric about the long axes of the ribbons, but the terminals of SiNRs break the symmetry. The DFT calculation results revealed a buckled single-layer structure of SiNRs, which is composed of Si hexagonal and tetragonal rings.

DOI: 10.1103/PhysRevMaterials.5.034002

I. INTRODUCTION

In recent years, progress in the development and miniaturization of high-functionality electronic devices has stimulated interest in one-dimensional materials. Graphene nanoribbons are the best-known and most widely researched one-dimensional materials. Depending on the crystallographic orientation of the edges, graphene nanoribbons have different electronic and magnetic behaviors [1,2]. Besides graphene nanoribbons, other nanoribbon materials, such as borophene nanoribbons [3], silicon carbon nanoribbons [4], and boron nitride nanoribbons [5] have also been studied.

Compared with the above-mentioned one-dimensional materials, silicon one-dimensional materials, such as Si nanotubes and Si nanoribbons (SiNRs), are more compatible with current Si-based electronics devices. SiNRs and silicon nanotubes with widths or diameters from several tens to several hundreds of nanometers have been successfully fabricated [6–8]. SiNR field-effect sensors have also been fabricated [9,10].

In recent years, theoretical and experimental studies have also investigated graphenelike SiNRs, which are composed of only a single layer of silicon atoms. Theoretical studies predicted that single-atomic-layer-thick SiNRs have several outstanding electronic properties, such as size-dependent energy band gaps [11,12], that are essential for application to field-effect transistors. Additionally, the magnetic properties of SiNRs, such as giant magnetoresistance [13,14] were reported, showing the potential for the application of SiNRs to future Si-based spintronic devices [15].

Experimentally, perfectly ordered SiNRs were found to form spontaneously on Ag(001) [16], Ag(110) [17–19], and Au(110) [20] surfaces. These SiNRs are commensurate with the substrate and are several angstroms or several nanometers in width. Among them, SiNRs on Ag(110) have been well investigated. Under scanning tunneling microscopy (STM) observation, SiNRs appeared as two or four rows of protrusions with a zigzag arrangement [21]; these are named single- and double-strand Si nanoribbons, respectively. The atomic structure of SiNRs on Ag(110) had remained an open question for a long time. Various different structural models were proposed for them. In 2016, a pentagon model was proposed based on the density functional theory (DFT) calculation [22]. After that, the pentagon model was confirmed by grazing-incidence x-ray diffraction [23], and Si pentagonal rings were successfully visualized by high-resolution atomic force microscopy (AFM) imaging [24]. Diverse experimental methods combined with theoretical calculations are important for determining the exact atomic structure of SiNRs on Ag(110).

On the other hand, Ag(111) has been widely used as a substrate for the epitaxial growth of silicene, which is a two-dimensional material composed of single-layer Si atoms with a hexagonal buckled structure [25–27]. Those studies found that deposited Si formed various superstructures on Ag(111), such as (4×4) [25] and $(\sqrt{13} \times \sqrt{13})R13.9^\circ$ phases [26]. Other Si structures, such as one-dimensional SiNRs, can also be expected to form on Ag(111). In the present paper, we report the self-assembled SiNRs on Ag(111). Here we present a synthesis method, the results of STM and AFM observations, and an atomic structure model based on the results of DFT calculations.

II. EXPERIMENT AND THEORY

All the experiments were carried out in ultra-high-vacuum conditions [(UHV); base pressure of $\sim 5 \times 10^{-9}$ Pa]. Before Si deposition, we cleaned an Ag(111) sample by Ar^+ ion sputtering and subsequent annealing at 600 °C for about 15 min.

*ysugimoto@k.u-tokyo.ac.jp

Then less than 1 monolayer (ML) of Si was deposited onto the prepared Ag(111) surface by holding it at 180 °C to form SiNRs. A Sb-doped Si(111) wafer (size: $6 \times 3 \times 0.5$ mm^3, electrical resistivity: 0.01 Ω cm) was used as the deposition source. The Si wafer and Ag(111) substrate used in this research were also used to form silicene in previous studies [28–30]. The synthesis difference between them are the temperature of Ag(111) during deposition (about 230 °C for silicene) and the flux of evaporated Si (more for silicene), i.e., less current is needed to flow through the Si wafer to form SiNRs.

The STM/AFM observation was carried out at both 4.8 K and room temperature in different UHV chambers. The STM/AFM observations at 4.8 K were conducted in an Omicron low-temperature STM/AFM system. A quartz tuning fork with an etched W tip was used for frequency modulation AFM [resonance frequency (f_0) of 26.2 kHz, spring constant (k) of 1800 N/m, quality factor of $\sim 2 \times 10^4$]. A CO molecule coadsorbed on the surfaces was picked up to attach to the tip apex [31]. AFM images were obtained in a constant height mode at sample bias $V_s = 0$ mV and an oscillation amplitude (A) of 0.10 nm. The origin of the tip height Δz is the set-point height determined by STM at $V_s = 30$ mV and tunneling current $I = 20$ pA over the bare Ag surface. The STM/AFM observations at room temperature were conducted in a custom-built STM/AFM system [32]. Commercial Pt-coated Si cantilevers, cleaned by Ar^+ ion sputtering, were used.

Low-energy electron diffraction was used to determine the crystallographic orientation of the Ag substrate.

DFT calculations within a generalized gradient approximation [33] were performed by using the OPENMX code [34] based on norm-conserving pseudopotentials generated with multireference energies [35] and optimized pseudoatomic basis functions [36]. For each Si atom, two, two, and one optimized radial functions were allocated for the s, p, and d orbitals, respectively, as denoted by $s2p2d1$. For the Ag atom, $s3p2d2$ basis functions were adopted. A cutoff radius of 7 bohr was chosen for the basis functions of Si and Ag atoms. A regular mesh of 220 Ry in real space was used for the numerical integrations and for the solution of the Poisson equation. One k point, the Γ point, was adopted to study a slab consisting of a nanoribbon on three Ag layers. The bottom Ag layer, whose coordinates were obtained by geometrical optimization of the bulk calculation, was kept fixed to simulate the bulk crystal termination of the surface. A $7 \times 1 \times 1$ mesh of k points was adopted for a periodic model of SiNRs. The periodic slab approach with a vacuum layer of about 20 Å was used to prevent interaction between periodic layers. The geometry was optimized using a threshold of 0.0003 Hartree/bohr for the forces.

The AFM simulations were conducted using the probe particle model [37] taking account of pairwise Lennard-Jones potentials together with electrostatic force between the tip and the sample [38]. To model a CO-decorated tip, we used a d_{z^2}-like quadrupole tip [39] with a bending stiffness of 0.25 N/m and a quadrupole moment of $-0.15\ e$Å^{-2}. The equilibrium position of the probe particle was set at 4 Å below the metal-tip apex. The stimulated images in the main text were obtained with the distance between the metal-tip apex and the topmost Ag atom of 11.2 Å. The details of the AFM simulations are described in the Supplemental Material [40].

III. RESULTS AND DISCUSSIONS

Figure 1(a) shows an STM image of the Ag(111) surface with Si deposition. This STM image was obtained at 4.8 K. Five one-dimensional ribbon structures (shown by blue arrows) are shown in this image. With the deposition of 1 ML of Si atoms onto Ag(111), the formation of silicene has been confirmed. Therefore, the one-dimensional ribbon structures shown are assumed to be SiNRs. Two of them align along the $[01\bar{1}]$ direction, two of them align along the $[10\bar{1}]$ direction, and the other one aligns along the $[1\bar{1}0]$ direction. SiNRs grow along these three equivalent directions because the Ag(111) substrate has a threefold symmetry about the [111] axis. The dark areas appear as mixtures of atoms that are assumed to be an alloy of silver and silicon.

Figures 1(b) and 1(c) show enlarged STM images of SiNRs obtained at 4.8 K. The SiNR in Fig. 1(b) is indicated by the black dotted rectangle in the overview image [Fig. 1(a)]. The enlarged STM images reveal more details of the atomic structure of SiNRs on Ag(111). Under STM observation, SiNRs appear as two rows of protrusions. SiNRs in Figs. 1(b) and 1(c) contain four pairs and two pairs of protrusions, respectively. Unlike the SiNRs on Ag(110), whose protrusions are in a zigzag arrangement under STM observation, the protrusion pairs of SiNRs on Ag(111) have a mirror symmetry about the long axis. Besides that, both SiNRs in Figs. 1(b) and 1(c) also contain two separate protrusions at each terminal [see green circles in Fig. 3(a)].

Figure 1(d) shows an STM image obtained at room temperature. It shows a SiNR consisting of ten pairs of protrusions. Under STM observation, the SiNRs observed at room temperature appear to be the same as those observed at 4.8 K. This indicates the stability of SiNRs even at room temperature.

In this paper, we observed more than 30 SiNRs, all having the same width and only differing in length. The observed shortest and longest SiNRs have lengths of 2 nm [Fig. 1(c)] and 9 nm (14 pairs of protrusions), respectively. STM was measured in the range of ±1000 mV. There was no significant change in appearance among SiNRs, indicating that STM resolved only geometrically protruded Si atoms.

In previous studies, high-resolution AFM imaging for silicene on Ag(111) [28–30] and SiNRs on Ag(110) [24] visualized all the constituent Si atoms, which provided solid evidence for atomic structure determinations. These studies motivated us to achieve high-resolution AFM imaging for SiNRs on Ag(111) to reveal the atomic structures of SiNRs. Figure 1(e) shows an AFM image of the SiNR shown in Fig. 1(b). This AFM image was measured in constant-height mode at 4.8 K. The tip was decorated by a CO molecule. The SiNRs under AFM observation showed a similar appearance to SiNRs under STM observations [Figs. 1(b)–1(d)]. This supports the above-mentioned interpretation that STM resolves the protruded Si atoms. The lateral and longitudinal distances of the protrusions measured from AFM images and STM images are almost the same: 0.57 ± 0.02 and 0.59 ± 0.02 nm, respectively. Here we note that the longitudinal distance is twice the lattice constant of the Ag(111) substrate.

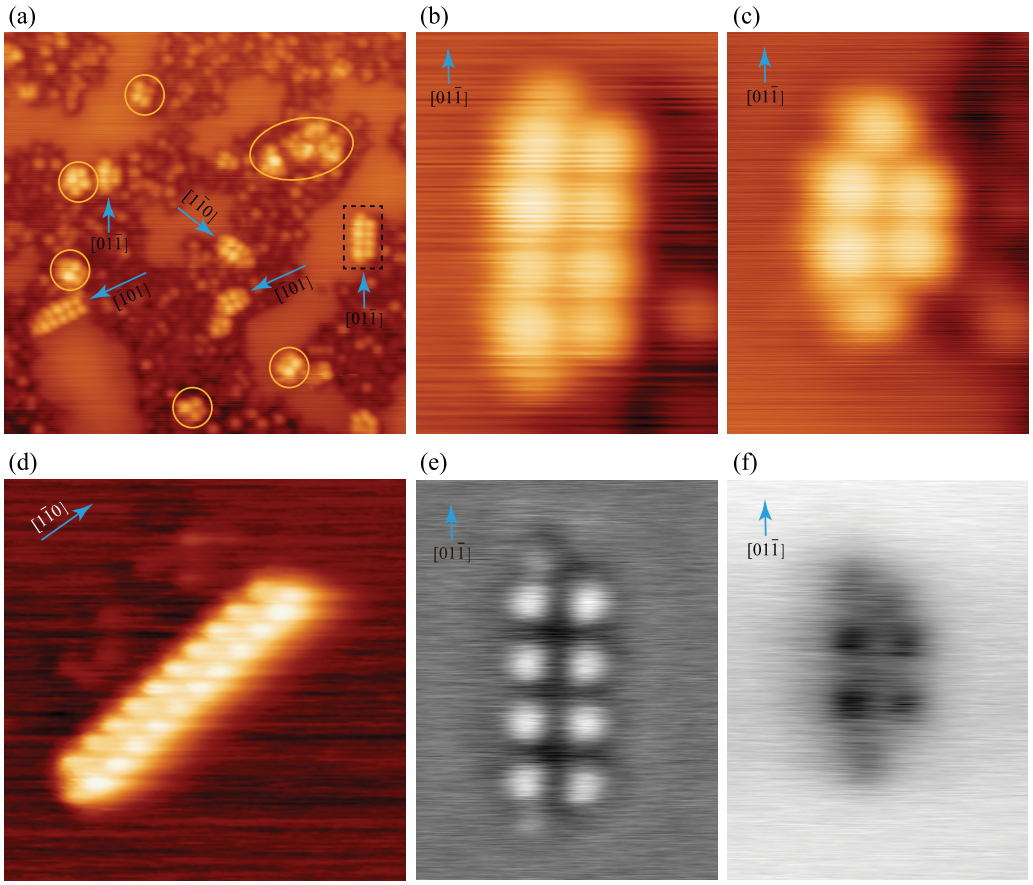

FIG. 1. (a)–(d) STM topography images of SiNRs. [(a) 25.0 × 25.0 nm^2, $V_s = 30$ mV, $I_t = 0.02$ nA, and 4.8 K. (b) and (c) 3.0 × 4.0 nm^2, $V_s = 30$ mV, $I_t = 0.02$ nA, and 4.8 K. (d) 8.0 × 8.0 nm^2, $V_s = -1000$ mV, $I_t = 0.03$ nA, room temperature.] (e) AFM image of SiNR shown in (b) working in a repulsive force regime [3.0 × 4.0 nm^2, $\Delta z = +50$ pm, 4.8 K, color-map white: 3.8 Hz, black: −3.1 Hz]. (f) AFM image of another SiNR working in an attractive force regime [3.0 × 4.0 nm^2, $\Delta z = +50$ pm, 4.8 K, color-map white:−12.4 Hz, black: −25.8 Hz].

This suggests that SiNRs are commensurate with the Ag(111) substrate.

AFM imaging in an attractive force regime was also carried out at 4.8 K with tips without CO decoration. Compared with the AFM image obtained in a repulsive force regime [Fig. 1(e)] where atomic features appear as more positive frequency shifts (Δf), the atomic features in the AFM image obtained in the attractive force regime [Fig. 1(f)] appear as more negative Δf. We found that the resolution of SiNRs on Ag(111) under AFM imaging in both repulsive [Fig. 1(e)] and attractive force regimes [Fig. 1(f)] is almost the same with STM. It is difficult to consider that these visualized Si atoms are all the constituent Si atoms of SiNRs. This is because the distances of the observed protrusions are much larger compared with Si-Si bond length. Under both STM and AFM, the lateral and longitudinal distances of visualized protrusions are 0.57 and 0.59 nm, respectively. However, the Si-Si bond length is 2.35 Å for the bulk Si; 2.28–2.31 Å, for silicene [41,42], and 2.35–2.37 Å for SiNRs on Ag(110) [22]. Such a Si-Si covalent bond would be essential to stabilize the Si nanostructures. Therefore, we assume that SiNRs on Ag(111) have invisible Si atoms that are located at the lower position rather than the STM/AFM-visible Si atoms. It is because if all of the constituent atoms are at the same height, AFM must resolve more. For these reasons, SiNRs should be composed of Si atoms with, at least, two different heights.

Based on the results of the STM and AFM observations, DFT calculations were performed to determine the exact atomic structure of the SiNRs on Ag(111). The atomic structure should satisfy the following conditions:

(1) SiNRs are commensurate with the $\langle 1\bar{1}0\rangle$ directions of Ag(111). The periodicity length of the structural unit is twice the lattice constant of Ag(111).

(2) The periodic units inside SiNRs have mirror symmetry about the $\langle 1\bar{1}0\rangle$ orientations of Ag(111).

(3) The constituent Si atoms of SiNRs must be of, at least, two different heights.

Based on the above conditions, an atomic structure model was proposed. It is shown in Fig. 2(a).

Figure 2(a) shows a SiNR with infinite length. In each periodic unit (represented by a green rectangle), there are eight Si atoms in a stacking structure. Six of these atoms are at relatively low positions and are not visualized by AFM or STM imaging. The other two Si atoms are supported by these low Si atoms and are at high positions; they correspond to the atomic features in the AFM and STM images. The left and right halves of the periodic unit are mirror symmetric. In each half of the periodic unit, three lower Si atoms and a higher one

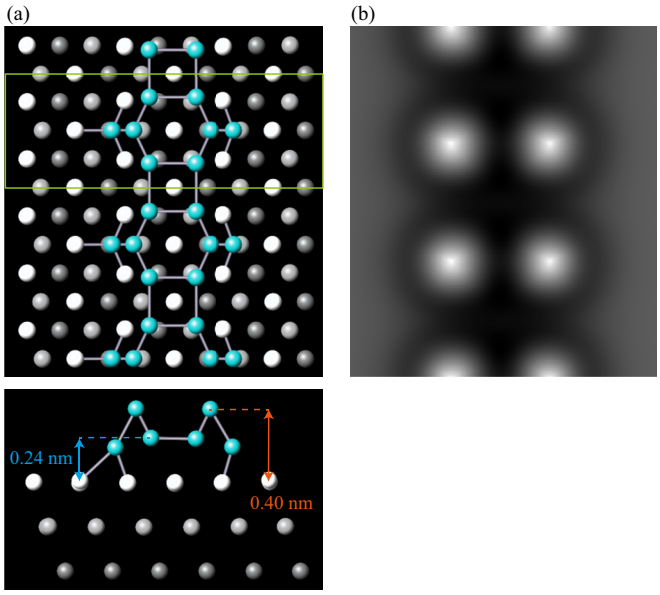

FIG. 2. (a) Top view (upper panel) and side view (lower panel) of repetition of calculated periodic unit model of SiNR. Blue circles represent Si atoms. The white, light-gray, and dark-gray circles represent the Ag atoms in the first, second, and third layers, respectively. (b) Simulated AFM image of the repeated periodic unit model of the calculated SiNR on Ag(111).

forming a pyramid structure can be regarded as the minimal structure unit of SiNRs. Its physical origin is that Si atoms prefer $sp3$ hybridization to $sp2$, which causes SiNRs have the buckled monolayer structure similar to silicene. These minimal structure units are positioned such that the highest Si atoms are above the Ag hollow site. The highest atoms of the minimal structure units on the left and right sides of SiNRs are above the hcp and fcc hollow sites, respectively. The pyramid vertices of four adjacent minimal structure units bond with each other, forming a Si tetragonal ring. In this structural model, the Si-Si bond length is 2.36–2.49 Å. It is in good agreement with above-mentioned Si-Si bond lengths in other Si structures. The whole SiNR is composed of Si hexagonal rings and tetragonal rings, which alternate with each other along the SiNR chain aligned along $\langle 1\bar{1}0\rangle$ orientations [Fig. 2(a)]. For this reason, the SiNR shown in Fig. 1(c) should be the shortest possible SiNR. Figure 2(b) shows the simulated AFM image of SiNR, which agrees well with the experimental AFM images [Fig. 1(e)].

In this structural model, the height difference between the higher Si atoms and the first-layer Ag atoms is about 0.40 nm. In contrast, the height difference between the lower Si atoms and the first-layer Ag atoms is about 0.24 nm. This large buckled height of about 0.16 nm should be the reason why we cannot visualize the lower Si atoms by AFM working in either a repulsive or an attractive force regime.

With the CO-decorated tip, high-resolution AFM imaging was achieved for SiNRs on Ag(110) [24]. The buckled height between higher and lower Si atoms of SiNRs on Ag(110) is 0.07 nm [22], which is much smaller than that of SiNRs on Ag(111). For this reason, it is very difficult for AFM with a CO-decorated tip to visualize more Si atoms of SiNRs on Ag(111) in this paper. This also is the case for the simulated AFM image [Fig. 2(b)].

On the other hand, high-resolution AFM imaging was reported for (4×4) [29], $(\sqrt{13} \times \sqrt{13})R13.9^\circ$ [28], and the T phase [30] of silicene on Ag(111). With AFM working in an attractive force regime, all the constituent Si atoms forming a honeycomb pattern are visualized. The high-resolution imaging mechanism was figured out in the studies of the $(\sqrt{13} \times \sqrt{13})R13.9^\circ$ phase [28]. In the case of the $(\sqrt{13} \times \sqrt{13})R13.9^\circ$ phase of silicene on Ag(111), the height difference between the topmost Si atoms and the lower Si atoms is about 0.09 nm. The lower Si atoms of silicene were pulled up by the attractive force with a tip. Thus, high-resolution AFM imaging was achieved. However, the high buckling of SiNRs causes a sharp bonding angle between the lower and the higher Si atoms. Moreover, four lower Si atoms form a tetragonal ring together, which gives the SiNRs a rigid structure. For these reasons, it is difficult for attractive AFM tips to affect these lower Si atoms.

We also compared the height differences between silicene and bare silver and that of SiNRs and bare silver. Under AFM measurements, the results for the silicene (4×4) phase and SiNRs are about 0.10 and 0.15 nm, respectively, indicating that the height of SiNRs should be larger than that of silicene. On the other hands, in a DFT-calculated model, the height of the highest silicene atoms and first-layer silver atoms is about 0.3 nm [28]. In our proposed atomic model for SiNRs, the height of the topmost Si atoms and first-layer silver atoms is about 0.4 nm. It is also in good agreement with the AFM results.

We also performed the calculations to investigate the electronic structure of SiNRs. The results show that the band structure of SiNR cross the Fermi level, and the interaction between SiNR and the Ag substrate is strong. The detailed results are shown in the Supplemental Material [40].

Besides this atomic structure model, we also performed calculations for other atomic structure models (see the Supplemental Material [40]). In the trial structural model shown in Fig. S1 of the Supplemental Material [40], there are two more Si atoms in each periodic unit (shown by arrows) compared with the proposed model shown in Fig. 2(a). However, this trial model did not converge during the structural optimization. In the trial structural model shown in Fig. S2 of the Supplemental Material [40], in each periodic unit, the two highest Si atoms are removed compared with structural model in Fig. 2(a). The stabilized atomic structure does not satisfy the condition that constituent Si atoms cannot be the same height. In the trial structural model shown in Fig. S3 of the Supplemental Material [40], the initial atomic structure of SiNR is the same as the finally proposed structure, but their relative positions with the Ag substrate are different. Here the highest Si atoms are at the top sites of the Ag substrate but not the hollow sites. The stabilized structure was flattened so that all the constituent Si atoms are at almost the same height, hence, it does not satisfy the condition mentioned above, either.

Another interesting characteristic of SiNRs is that, under STM and AFM observations, the attachment atoms are always located on the single side of SiNR terminals [Figs. 1(a)–1(f)

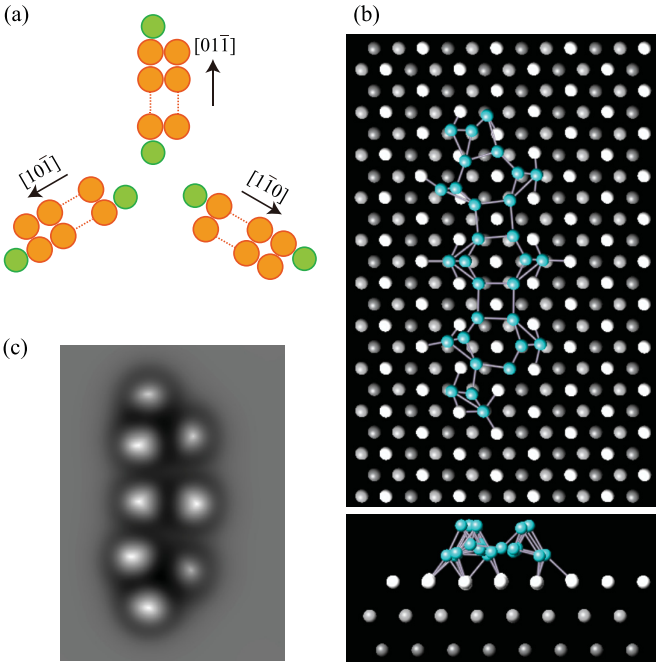

FIG. 3. (a) Schematic of the attachment atoms of SiNRs. (b) Top view (upper panel) and side view (lower panel) of calculated stable structure model of SiNR. The blue circles represent Si atoms. The white, light-gray, and dark-gray circles represent the Ag atoms in the first, second, and third layers, respectively. (c) Simulated AFM image of the calculated SiNR on Ag(111).

and 3(a)], which breaks the symmetry of SiNR about the long axis. In STM and AFM images, these attachment atoms are located slightly towards the center axis of SiNRs compared with the Si atoms forming the periodic units. Considering the asymmetry of Ag(111) crystal about the $\langle 1\bar{1}0\rangle$ orientations, the second-layer Ag atoms of the substrate should influence the position of the attachment atoms. The DFT calculation was also carried out to reveal the asymmetric attached Si atoms at the terminals of SiNRs. Figures 3(b) and 3(c) show a stable structure and the simulated AFM image of a SiNR composed of three periodic unit and attachment atoms. In the calculated stable structure, the terminal of SiNRs are composed of four Si atoms in which the highest Si atom is supported by the other three Si atoms. These four Si atoms form the pyramidal structure, which is the same as the minimal structure unit in the body of SiNRs. The highest Si atoms are located on the silver hcp hollow sites. The simulated AFM image [Fig. 3(c)] well reproduces the experimental AFM images. The atomic structure that attached Si atoms are at the positions that are opposite to the positions of attached atoms in Fig. 3, that is, the highest Si atoms of the pyramid structure are above the silver fcc hollow sites are also calculated. The result shows that, in this case, SiNR structure cannot be stable and collapses into a cluster structure.

IV. SUMMARY

In conclusion, this paper presented a new one-dimensional material, SiNR on Ag(111), that is, stable under room temperature. We investigated it by STM, AFM, and DFT calculations. We proposed its atomic structure, which is composed of Si hexagonal and tetragonal rings. Under STM and AFM observations, attachment Si atoms always locate on the terminals of SiNRs, which was also explained by DFT calculations. We believe that this paper will help to reveal the interesting electronic properties of SiNRs on Ag(111) in future works. We also expect that our results can promote the fabrication of analogous Si low-dimensional structures on other surfaces with outstanding properties, such as size-dependent energy band gaps, which are predicted in the calculation studies, as well as their application in future electronic devices.

ACKNOWLEDGMENTS

This work was supported by JSPS KAKENHI Grants No. JP18H03859, No. JP18H01807, No. JP18K18990, and No. JP20H05178. Y.S. acknowledges the support of the Asahi Glass Foundation and Toray Science Foundation.

[1] Y.-W. Son, M. L. Cohen, and S. G. Louie, Nature (London) **444**, 347 (2006).
[2] P. Koskinen, S. Malola, and H. Häkkinen, Phys. Rev. Lett. **101**, 115502 (2008).
[3] Q. Zhong, L. Kong, J. Gou, W. Li, S. Sheng, S. Yang, P. Cheng, H. Li, K. Wu, and L. Chen, Phys. Rev. Materials **1**, 021001(R) (2017).
[4] P. Lou and J. Y. Lee, J. Phys. Chem. C **113**, 12637 (2009).
[5] H. Zeng, C. Zhi, Z. Zhang, X. Wei, X. Wang, W. Guo, Y. Bando, and D. Golberg, Nano Lett. **10**, 5049 (2010).
[6] D. F. Perepichka and F. Rosei, Small **2**, 22 (2006).
[7] Y. Qiu, H. Bender, O. Richard, M.-S. Kim, E. Van Besien, I. Vos, M. D. P. De Ten Broeck, D. Mocuta, and W. Vandervorst, Sci. Rep. **5**, 12692 (2015).
[8] W. Shi, H. Peng, N. Wang, C. P. Li, L. Xu, C. S. Lee, R. Kalish, and S.-T. Lee, J. Am. Chem. Soc. **123**, 11095 (2001).
[9] A. Tarasov, W. Fu, O. Knopfmacher, J. Brunner, M. Calame, and C. Schönenberger, Appl. Phys. Lett. **98**, 012114 (2011).
[10] Z. Bao, J. Sun, X. Zhao, Z. Li, S. Cui, Q. Meng, Y. Zhang, T. Wang, and Y. Jiang, Int. J. Nanomed. **12**, 4623 (2017).
[11] S. Cahangirov, M. Topsakal, E. Aktürk, H. Şahin, and S. Ciraci, Phys. Rev. Lett. **102**, 236804 (2009).
[12] X.-T. An, Y.-Y. Zhang, J.-J. Liu, and S.-S. Li, Appl. Phys. Lett. **102**, 213115 (2013).
[13] C. Xu, G. Luo, Q. Liu, J. Zheng, Z. Zhang, S. Nagase, Z. Gao, and J. Lu, Nanoscale **4**, 3111 (2012).
[14] J. Kang, F. Wu, and J. Li, Appl. Phys. Lett. **100**, 233122 (2012).
[15] Y. Ding and J. Ni, Appl. Phys. Lett. **95**, 083115 (2009).
[16] C. Léandri, H. Oughaddou, B. Aufray, J. Gay, G. Le Lay, A. Ranguis, and Y. Garreau, Surf. Sci. **601**, 262 (2007).
[17] B. Aufray, A. Kara, S. Vizzini, H. Oughaddou, C. Léandri, B. Ealet, and G. Le Lay, Appl. Phys. Lett. **96**, 183102 (2010).

[18] C. Leandri, G. Le Lay, B. Aufray, C. Girardeaux, J. Avila, M. Davila, M. Asensio, C. Ottaviani, and A. Cricenti, Surf. Sci. **574**, L9 (2005).
[19] P. De Padova, O. Kubo, B. Olivieri, C. Quaresima, T. Nakayama, M. Aono, and G. Le Lay, Nano Lett. **12**, 5500 (2012).
[20] M. Rachid Tchalala, H. Enriquez, A. J. Mayne, A. Kara, S. Roth, M. G. Silly, A. Bendounan, F. Sirotti, T. Greber, B. Aufray *et al.*, Appl. Phys. Lett. **102**, 083107 (2013).
[21] B. Feng, H. Li, S. Meng, L. Chen, and K. Wu, Surf. Sci. **645**, 74 (2016).
[22] J. I. Cerdá, J. Sławińska, G. Le Lay, A. C. Marele, J. M. Gómez-Rodríguez, and M. E. Dávila, Nat. Commun. **7**, 13076 (2016).
[23] G. Prévot, C. Hogan, T. Leoni, R. Bernard, E. Moyen, and L. Masson, Phys. Rev. Lett. **117**, 276102 (2016).
[24] S. Sheng, R. Ma, J.-b. Wu, W. Li, L. Kong, X. Cong, D. Cao, W. Hu, J. Gou, J.-W. Luo *et al.*, Nano Lett. **18**, 2937 (2018).
[25] P. Vogt, P. De Padova, C. Quaresima, J. Avila, E. Frantzeskakis, M. C. Asensio, A. Resta, B. Ealet, and G. Le Lay, Phys. Rev. Lett. **108**, 155501 (2012).
[26] C.-L. Lin, R. Arafune, K. Kawahara, N. Tsukahara, E. Minamitani, Y. Kim, N. Takagi, and M. Kawai, Appl. Phys. Express **5**, 045802 (2012).
[27] B. Feng, Z. Ding, S. Meng, Y. Yao, X. He, P. Cheng, L. Chen, and K. Wu, Nano Lett. **12**, 3507 (2012).
[28] L. Feng, K. Yabuoshi, Y. Sugimoto, J. Onoda, M. Fukuda, and T. Ozaki, Phys. Rev. B **98**, 195311 (2018).
[29] J. Onoda, K. Yabuoshi, H. Miyazaki, and Y. Sugimoto, Phys. Rev. B **96**, 241302(R) (2017).
[30] J. Onoda, L. Feng, K. Yabuoshi, and Y. Sugimoto, Phys. Rev. Materials **3**, 104002 (2019).
[31] L. Gross, F. Mohn, N. Moll, P. Liljeroth, and G. Meyer, Science **325**, 1110 (2009).
[32] Y. Sugimoto, Y. Nakajima, D. Sawada, K.-i. Morita, M. Abe, and S. Morita, Phys. Rev. B **81**, 245322 (2010).
[33] J. P. Perdew, K. Burke, and M. Ernzerhof, Phys. Rev. Lett. **77**, 3865 (1996).
[34] T. Ozaki *et al.*, OPENMX package [http://www.openmx-square.org/].
[35] I. Morrison, D. M. Bylander, and L. Kleinman, Phys. Rev. B **47**, 6728 (1993).
[36] T. Ozaki, Phys. Rev. B **67**, 155108 (2003).
[37] P. Hapala, G. Kichin, C. Wagner, F. S. Tautz, R. Temirov, and P. Jelínek, Phys. Rev. B **90**, 085421 (2014).
[38] P. Hapala, R. Temirov, F. S. Tautz, and P. Jelínek, Phys. Rev. Lett. **113**, 226101 (2014).
[39] P. Hapala, M. Švec, O. Stetsovych, N. J. Van Der Heijden, M. Ondráček, J. Van Der Lit, P. Mutombo, I. Swart, and P. Jelínek, Nat. Commun. **7**, 11560 (2016).
[40] See Supplemental Material at http://link.aps.org/supplemental/10.1103/PhysRevMaterials.5.034002 for details of the AFM simulations and the trial structure models.
[41] C.-C. Liu, W. Feng, and Y. Yao, Phys. Rev. Lett. **107**, 076802 (2011).
[42] K. Kawahara, T. Shirasawa, R. Arafune, C.-L. Lin, T. Takahashi, M. Kawai, and N. Takagi, Surf. Sci. **623**, 25 (2014).